COMPRESSED DETECTION VIA MANIFOLD LEARNING

Hyun Jeong Cho, Kuang-Hung Liu, Jae Young Park

Email : { zzon, khliu, jaeypark } @umich.edu

1. INTRODUCTION

In many imaging applications such as Computed Tomography (CT) in medical imaging and Synthetic Aperture Radar (SAR) imaging, the collected raw data, residing in $\mathbb{R}^M$, of the receiver or detector can be modeled as data lying in the Fourier space of the target reflectivity function. The magnitude of the reflectivity is considered as the image of the target, and we are often interested in detecting specific features in the image, e.g. tumor in medical imaging and military weapons in SAR imaging. A natural way to achieve this goal is to form an image in $\mathbb{R}^N$, where $N > M$, and detect the feature in the spatial domain.

Recent development of a theory in [1] states that under certain conditions, random linear projections, $\Phi : \mathbb{R}^N \mapsto \mathbb{R}^L$, guarantees, with high probability, that all pairwise Euclidean and geodesic distances between points on $\mathcal{M} \subset \mathbb{R}^N$ are well preserved under the mapping Φ. This made us wonder if the geodesic distances of the original image, $\mathbb{R}^N$, and the corresponding raw data, $\mathbb{R}^M$, in SAR imaging were also reasonably preserved. Motivated by satisfactory results of simple tests to check this, which will be discussed in more detail later, we tried to detect features directly from the lower dimensional, or compressed, SAR raw data, without involving any image reconstruction step.

In this report, manifold learning techniques are applied to reduce the dimension of the raw data, and is followed by a detection step to achieve our goal. The theoretical framework will be discussed later in more detail. To our best knowledge, there has not yet been a successful image detection or classification algorithm that takes advantage of this framework and works directly on the domain where the raw data resides in. Since existing algorithms work in the spatial domain, the algorithms first have to transform the raw data to the spatial domain. This transformation step could be time consuming, and in general results in loss of information. Also, working with M dimensional data will be computationally less demanding. Thus, it is interesting to look at the problem of working directly on the raw data.

The rest of the report is structured as follows. First, technical background such as the theoretical framework mentioned above, the Laplacian Eigenmaps as a method of dimensionality reduction, and semi-supervised learning algorithm will be discussed. Carrying on, experimental results will be presented. Finally, we will conclude this report by giving discussion on the challenges and future works.

2. TECHNICAL BACKGROUNDS

2.1. Data Format Collected by SAR System

The radar is transmitting a narrow band linear FM signal at viewing angle θ, and the target reflectivity collected by the radar is demodulated to produce the SAR output data (complex value) [2].

It can be shown that the output data is the Fourier transform of the projection function of the target at angle θ, and by *Projection slice theorem* this equal to values of the two-dimensional Fourier transform of the target reflectivity function along a line in the Fourier plane that lies at angular orientation θ with respect to the X axis. Furthermore, the output data only contains Fourier data value in the bandwidth same as the transmitted FM signal. In summary, the collected data lies on the polar grid in the Fourier space. In reconstructing the image, one approach is to first interpolate the data from the polar grid to Cartesian grid, then perform the inverse FFT. An example of the collected data and interpolated data is shown in Fig. 1.

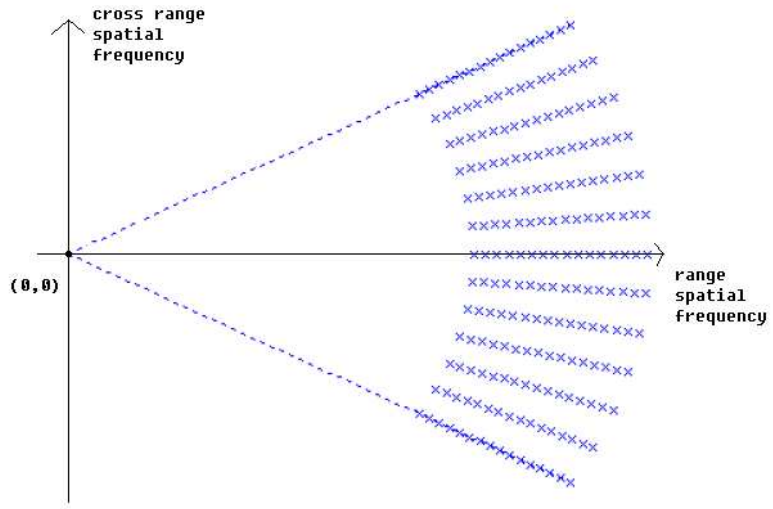

Fig. 1. Typical SAR data grid lying on a polar grid in the Fourier space

In the examples we considered, we want the coverage of the Cartesian data to encompass the spread of the SAR collected data which is lying on the polar grid. And we want it to be dense enough so the information loss due to the interpolation operation is minimum. The result of the interpolation is that we have to process more data than what the SAR system has collected.

2.2. Low Dimensional Manifold Learning

The aim of manifold learning is to discover some information about the structure of a manifold based on a collection of samples from it. Usually, the data presented is in $\mathbb{R}^N$ and the

learning is a nonlinear mapping from $\mathbb{R}^N$ to $\mathbb{R}^K$, for some $N > M > K$. Depending on the size of N, the process of obtaining and storing a large number of samples from a manifold may be very difficult. Also, manifold learning algorithms applied to data of large N may suffer from significant computational load. However, Theorem 3.1 and Corollary 3.1 presented in [1] imply that many of the properties of a manifold that one may wish to learn from data in $\mathbb{R}^N$ are approximately preserved in its image under a random projection to $\mathbb{R}^M$. To be more specific, it states that under a certain condition, with high probability, all pairwise distances between points on a submanifold are well-preserved up to a constant scaling factor under random linear projection. This property and a few others stated in [1] are desirable for manifold learning algorithms. Thus, it suggests that one can apply such learning algorithms to random projections of the original data and get a reasonable approximation to the true answer. This enables us to skip the reconstruction step of forming the original image from the raw data, which is an unnecessary, lossy, time consuming step when the primary aim is to detect a specific feature.

Motivated by this fact, we will assume the partial Fourier data obtained in SAR imaging to be random projections, $\Phi : \mathbb{R}^N \mapsto \mathbb{R}^M$, where Φ is the random projection operator, of the original image. This means that the partial Fourier data lives on the randomly projected manifold of the original image manifold. We will see in the subsequent sections that this is in fact a reasonable assumption, at least for the toy problems discussed in this report. With this assumption, we will apply manifold learning algorithms to this lower dimensional data to map them into even lower K dimensional domain.

2.3. Laplacian Eigenmaps

Laplacian Eigenmaps is a nonlinear dimensionality reduction technique that preserves locality and suggests clusters in a natural way. It explicitly considers the structure of the manifold on which the data might possibly reside.

Suppose we are given n points $x_1, \ldots, x_n \in \mathbb{R}^N$. We assume that the data lives on a lower dimensional manifold $\mathcal{M}$, and we wish to find a lower dimensional representation $y_1, \ldots, y_n \in \mathbb{R}^M$ where $M < N$. We construct a weighted graph with n nodes and edges connecting neighboring nodes. The edge connecting node i and j are assigned with weights $w_{i,j} \in [0, 1]$, where 1 represents self connection and 0 represents no connection. The data mapped into lower dimension is then represented by the eigenvectors of the graph Laplacian. The steps are described in more detail in the following.

1. Construct the connection matrix.
   Find the $n_n \in \mathbb{N}$ nearest neighbors of each node and connect the neighboring nodes with an edge. The closeness of two data is determined by the Euclidean distance. Note that nodes i and j are connected if node i is among the n_n nearest neighbors of node j or vice versa.[1]

2. Assign weights to each edge.
   We consider two ways of determining weights.

[1] Instead of choosing fixed number of nearest neighbors for each node, we can choose the neighbors whose distance from a node is not greater than some threshold. However, this often leads to graphs with several connected components and it is difficult to choose the threshold. [3]

(a) Heat kernel : $w_{i,j} = \exp\{-\frac{\|x_i - x_j\|^2}{t}\}$ where $t \in (0, \infty)$

(b) Constant weights : assign 1 to all edges.

Note that as $t \to \infty$, the Heat kernel approaches to a constant value.

3. Eigenmap.
Assuming that the graph is connected, compute the eigenvalues and eigenvectors of the graph Laplacian $L = D - W$, where D is a diagonal matrix with $D_{i,i} = \sum_j w_{i,j}$ and W is the matrix of weights $w_{i,j}$'s. Let $0 = \lambda_1 \leq \lambda_2 \leq \ldots \leq \lambda_n$ be the eigenvalues and let v_i be the eigenvector corresponding to λ_i, for $i = 1, \ldots, n$. Then the eigenvectors $v_2, \ldots, v_{M+1}$ represent the mapping of the data into $\mathbb{R}^M$:

$$x_i \to y_i = (v_2(i), \ldots, v_{M+1}(i)), \quad \forall i = 1, \ldots, n.$$

If the graph is not connected, compute the mapping for each connected component.

2.4. Detection and Classification using Semi-Supervised Learning algorithm

The problem is formulated in the following manner. We have a set of images, and only a partial set of images are labeled 1 or -1. We want to label the rest of the unlabeled images. Ultimately, we want to classify the whole data set.

We adopt the classification algorithm in [4], which tries to approximate the best classification by linear combination of the eigenvectors of the Laplacian. The procedure of the algorithm is described as follow:

Step 1: Construct the adjacency graph with n nearest neighbors. The distance can be the standard Euclidean distance or some other distance.

Step 2: Compute p eigenvectors E corresponding to the smallest eigenvalues for the eigenvector problem $Le = \lambda e$, where $L = W - D$ is the graph Laplacian for the adjacency graph. Assume we have k test images, the structure of E is as follows.

$$E = \begin{bmatrix} e_{11} & e_{12} & \cdots & e_{1k} \\ e_{21} & e_{22} & \cdots & e_{2k} \\ \vdots & \vdots & \ddots & \vdots \\ e_{p1} & e_{p2} & \cdots & e_{pk} \end{bmatrix}$$

Step 3: Building the classifier. Approximate the classifier by minimizing the error function:

$$Err(a) = \sum_{i=1}^{s} \left(c_i - \sum_{j=1}^{p} a_j e_{ji} \right)^2$$

where $a_j's$ are the coefficients we seek. s is the number of labeled data and $c_i's$ are the corresponding label. The solution is given by

$$a = (E_{lab}^T E_{lab})^{-1} E_{lab}^T c$$

where $c = (c_1, \cdots), c_s$ and

$$E_{lab} = \begin{bmatrix} e_{11} & e_{12} & \cdots & e_{1s} \\ e_{21} & e_{22} & \cdots & e_{2s} \\ \vdots & \vdots & \ddots & \vdots \\ e_{p1} & e_{p2} & \cdots & e_{ps} \end{bmatrix}$$

Step 4: Classifying unlabeled points. For unlabeled data x_i, we let the label c_i be

$$c_i = \begin{cases} 1, & if \ \sum_{j=1}^{p} a_j e_{ji} \geq 0 \\ -1, & if \ \sum_{j=1}^{p} a_j e_{ji} < 0 \end{cases}$$

3. SIMULATION

3.1. Experiment Road Map

We have first applied dimensionality reduction techniques to simple, full N dimensional image data. The images will be described in the subsequent section. Then, we have carried out the same simulation procedure with Fourier data of the images. This was basically just to test if our dimensionality reduction methods worked correctly in both spatial and Fourier domain. To imitate, naively, SAR imaging system, we have then taken the partial Fourier data and applied dimensionality reduction techniques to them. Since, the raw data obtained in SAR imaging are concentrated in high frequency region in Fourier domain, we have taken block portions of full Fourier data in high frequency range.

Once the results were satisfactory we repeated the above described procedure with more complicated, better imitations of real SAR data.

The data that we believe to be closest to the realistic situation tested in this report are raw SAR data with noise and random phase.

3.2. Test Data

The test images that we tried out were 64-by-64 images containing simple features. Examples from each class of images are shown in Figure 2. Each image of the same class are random shifts of the same image in x and y directions except for the noisy images. This results in a data set that lives on a two-dimensional manifold embedded in $\mathbb{R}^{64\times 64}$.

As mentioned above, 64-by-64 discrete Fourier transform of the test images and block portions of the Fourier data of the images in figure 2 were also tested. When testing with figure 2 (e) and (f) the manifold will no longer be a two dimensional manifold but a higher dimensional manifold due to noise. This is a more realistic image than the others because in reality we would have such noise components added to our original image.

Figure 3 gives you an idea what the raw SAR data looks like. Figure 3 (a) is a raw SAR data collected from an image patch containing small square reflector embedded on a noisy clutter. The raw SAR data is collected for several radial sample points and angular sample points. It resides on a polar grid in the Fourier domain as mentioned in Section 2, so it needs to be interpolated onto a Cartesian grid, where the interpolated SAR data is shown in Fig. 3

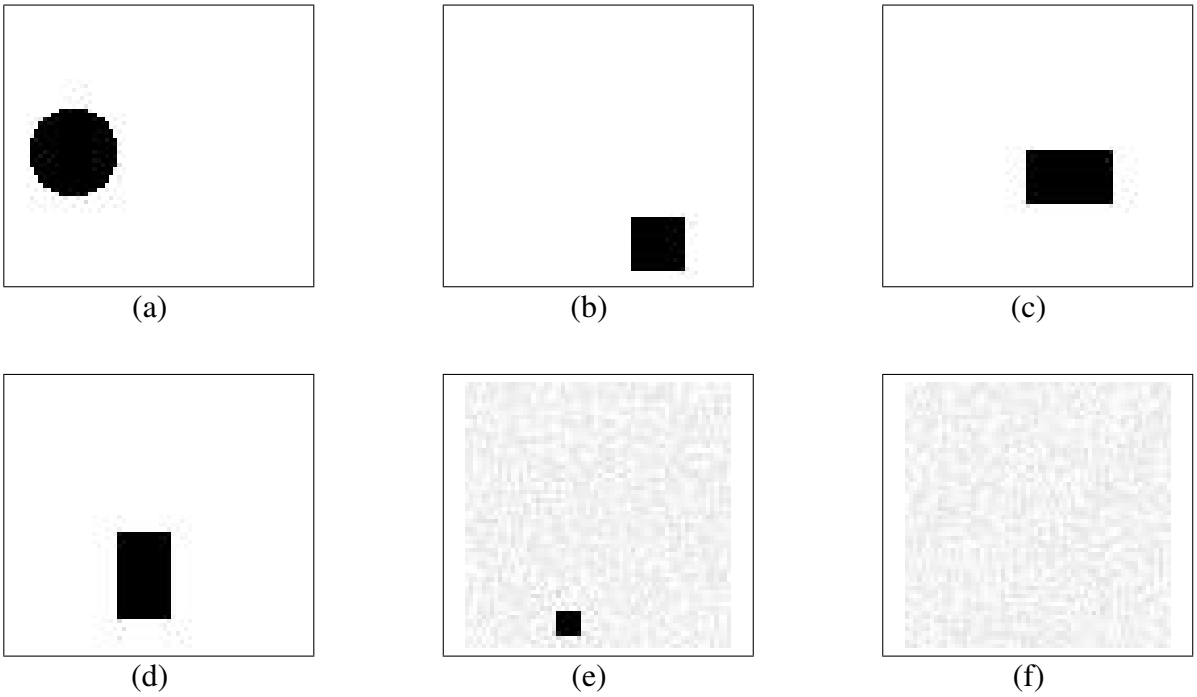

Fig. 2. Test Images. (a) Circle (b) Square (c) Horizontal bar (d) Vertical bar (e) Small square in noise (f) Noise

(b). Then the image, i.e. the magnitude of the complex-valued reflectivity, can be obtained by performing inverse Fourier transform. The image corresponding to the raw data shown in Fig. 3 (a) is shown in Fig. 3 (c). This is the data that matches closest to real SAR imaging data in this report.

3.3. Testing for Embedding

Our motivation discussed previously, to view the lower dimensional manifold where the raw data resides in, as a randomly projected manifold of the original image manifold is not exactly the case in SAR imaging. The actual manifold that the raw data resides in does not coincide with the randomly projected manifold. We have carried out tests to see if the theorem in [1] mentioned earlier supports the case of SAR data thinking of its manifold as one of the randomly projected manifold of the manifold that the original image resides in.

We note the reader that real SAR data must be purchased and even for toy images it is not easy to generate raw SAR data. When we tested whether or not the geodesic distances of the image manifold were preserved up to a scaling factor in the lower dimensional embedding of the raw data, we have used data that imitated closely the raw SAR data. To be more specific, we generated n images and also their block portions in high frequency range. With those two sets of data, we have tested for preservance of geodesic distances.

We repeated this with different types of images. The histogram in figure 4 is a histogram of the ratios of the geodesic distances of the original and partial data of all data points. The difference in the two histogram is the way we chose the partial Fourier data. Figure 4 a)

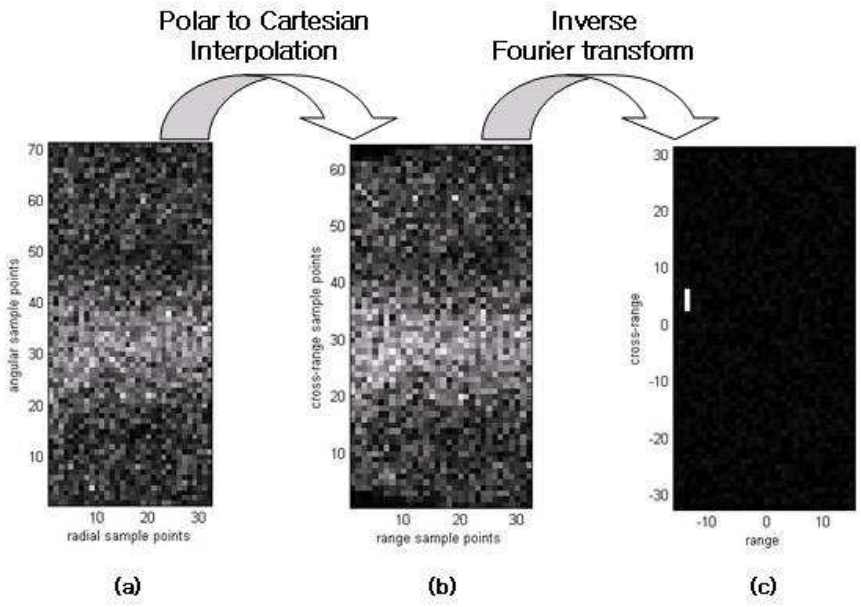

Fig. 3. SAR data description

the partial data was obtained by random projections, meaning we created an i.i.d. Gaussian random matrix of M-by-N and applied it to our image. The partial data in Figure 4 b) is the block portion of its Fourier data. We notice that the spread in values are in both cases about 0.2 with a high peak in the middle, which indicates that the all pointwise geodesic distances are reasonably preserved.

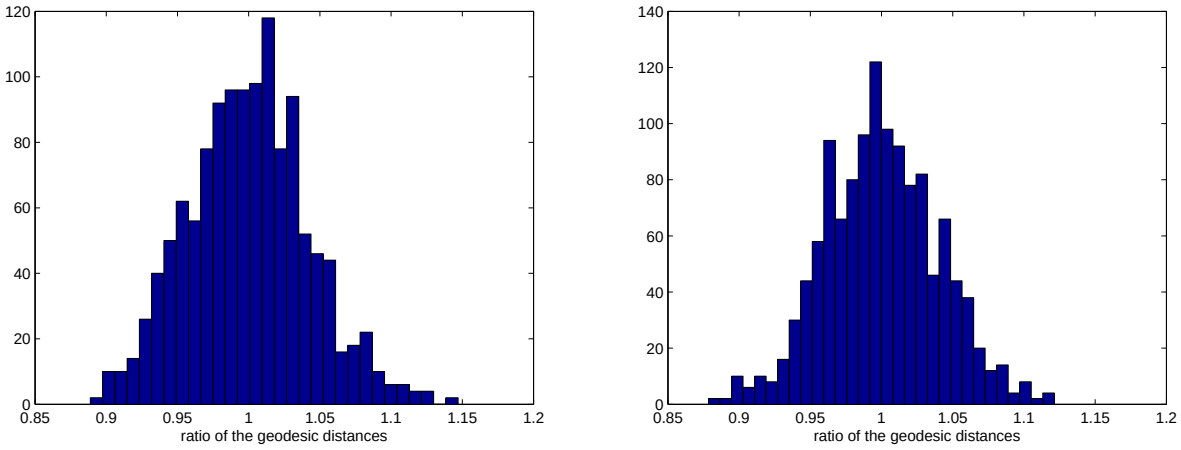

Fig. 4. Histogram of the ratio of the geodesic distances. (a) Ratio of the geodesic distances in a randomly projected domain to the geodesic distance in the original image domain. (b) Ratio of the geodesic distances in a block portion of the Fourier domain to the geodesic distance in the original image domain.

3.4. Simulation Procedure

We have first tested the above explained algorithm assuming full knowledge of the data's labels. The procedure is summarized below.
First, we chose two different classes of images, e.g. vertical bar and horizontal bar, and also decided on the number of images n to be taken from each class. Second, we set the free parameters such as the number of neighbors n_n and the value of t. Third, we have columnized 64-by-64 images into one single column and made a matrix of dimension (64×64)-by-n by stacking all n such columns side by side. Fourth, using this matrix, we applied the Laplacian Eigenmap algorithm to obtain the lower dimensional representations of the images.

Since Laplacian Eigenmaps has been proposed for semi-supervised learning [3],we have repeated the same experiment but this time assuming only partial knowledge of the data's labels. We used the detection algorithm described earlier on the lower dimensional representation as a means to classify the data into two classes.

3.5. Simulation Results

3.5.1. Dimensionality Reduction by Laplacian Eigenmap

Figure 5 shows a plot of two dimensional representation of hundred horizontal bars and hundred vertical bars of size 40-by-40. There is some sort of a pattern associated with images and its location of plot in this figure. Probably the most interesting two points will be the rightmost point among the circles tagged with its image and the upper leftmost point among the triangles also tagged by its image. Looking at these two images we realize that they in fact look very similar, most of the areas overlapping with each other, thus lying very closely to each other. We can also see that within the circles, moving up implies that the rectangles move up and moving down implies the opposite. Furthermore, moving left implies that the rectangles move to the right and moving right implies the opposite. For the triangles, we can also infer a similar pattern.

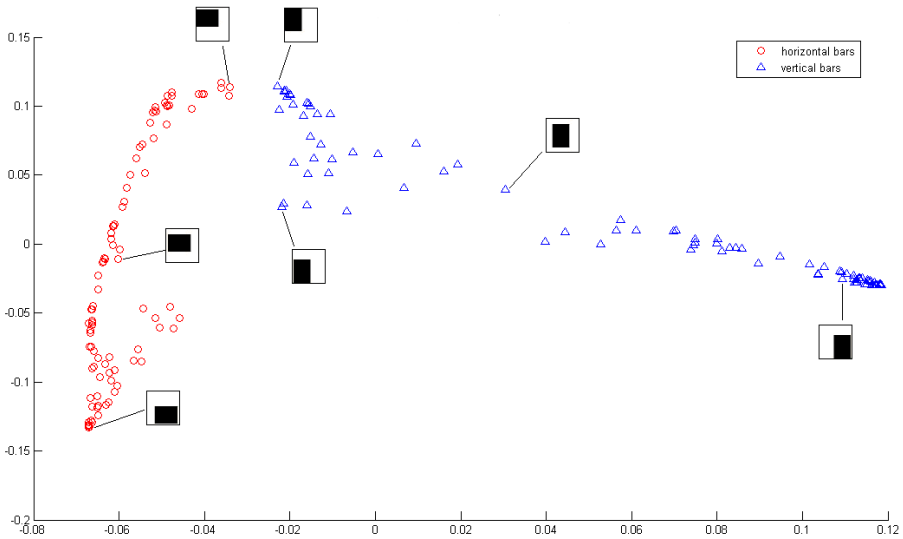

Fig. 5. Partial Fourier data mapped into $\mathbb{R}^2$

Figure 6 is the same plot as Fig. 5 but showing connected points in the Laplacian Eigenmaps.

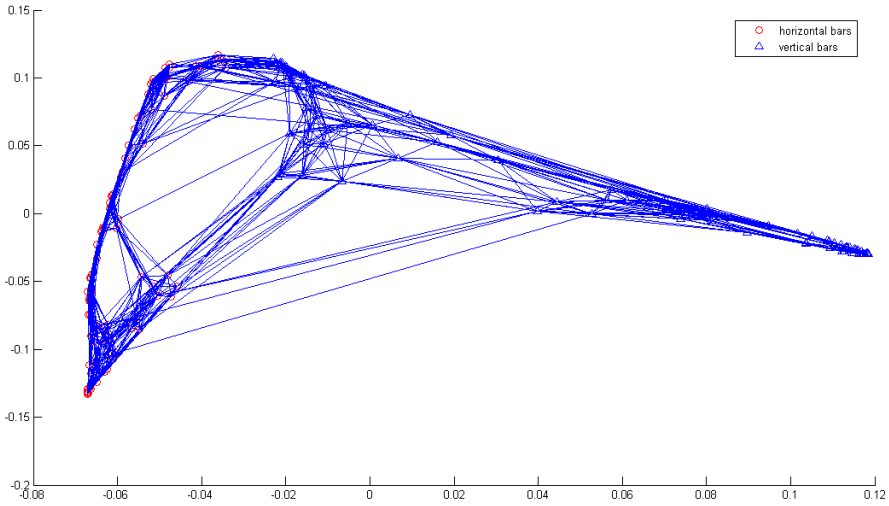

Fig. 6. Partial Fourier data mapped into $\mathbb{R}^2$ with neighboring edges

3.5.2. Model Selection Problem

Figure 7 illustrates the importance of choosing the value of the free parameters. Here, the data is composed of 500 circle images and 500 square images and $t = \infty$ is fixed. Figure 7 (a) shows the result when the number of nearest neighbors $n_n = 3$. Here, the graph is disconnected into four components and the feature extraction is not done as desired. Multiple squares and circles are overlapped with each other making it impossible to cluster them. Figure 7 (b) shows the result corresponding to $n_n = 7$, and the two classes of images form disjoint clusters. Lastly, Fig. 7 (c) shows the result corresponding to $n_n = 15$. The graph is highly connected, i.e. the weight matrix is noisy, and the low dimensional representation of the data have correspondingly high variance, thus not separable.

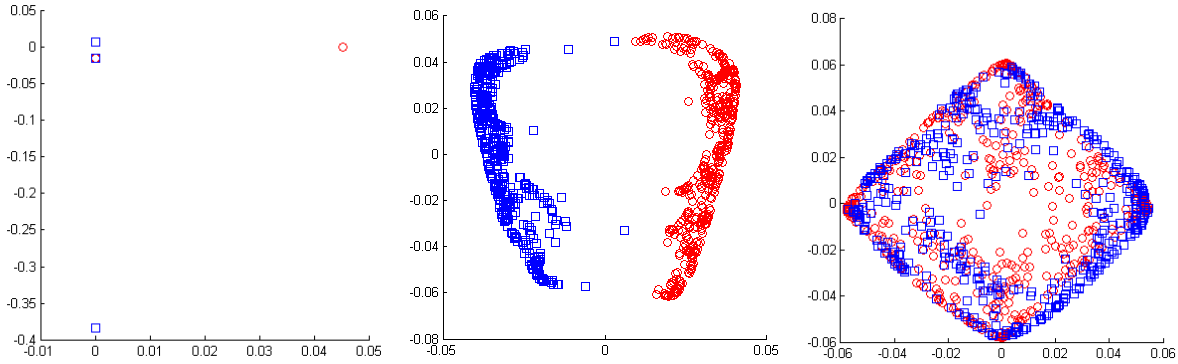

(a) $n_n = 3$ (b) $n_n = 7$ (c) $n_n = 15$

Fig. 7. Images (Circles and Squares) mapped into $\mathbb{R}^2$. $t = \infty$

3.5.3. Semi-supervised Learning

Figure 8 shows the results of dimensionality reduction and semi-supervised learning. The data was of partial Fourier data composed of 300 horizontal bars and 300 vertical bars. We assigned labels to only 20 data for each class, thus the labels of 560 data were unknown. The two-dimensional representation of the data were then clustered using K-means clustering and the labels of each cluster was determined via majority vote. Two horizontal bars depicted in ovals in the figures were misclassified as vertical bars.

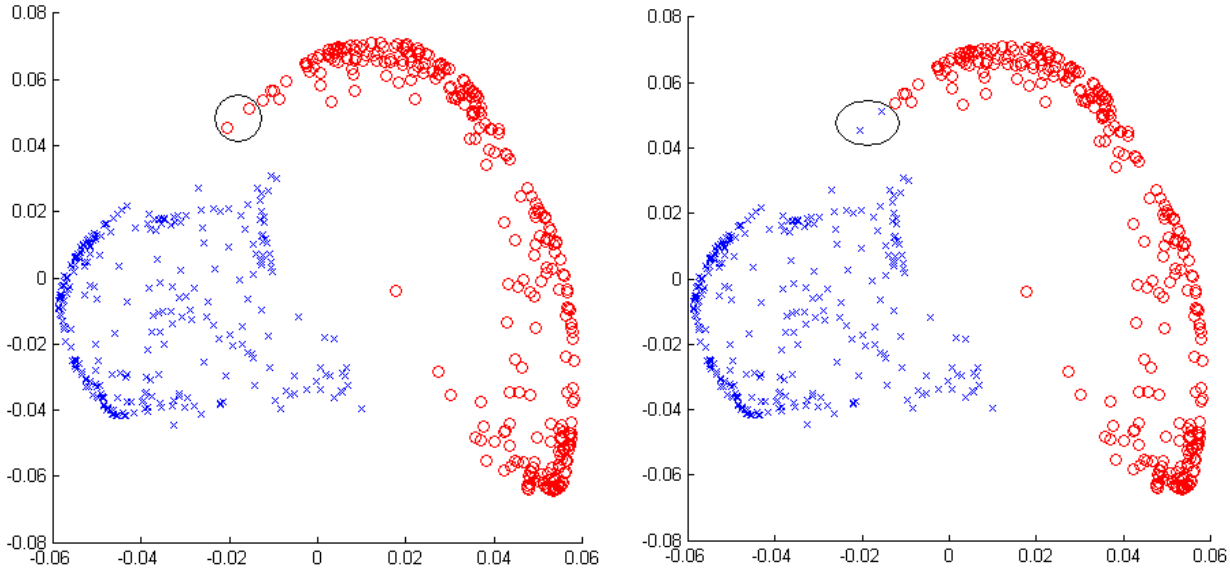

Fig. 8. Semi-supervised Learning. Circles correspond to horizontal bars and crosses correspond to vertical bars. (a) Partial Fourier data mapped into $\mathbb{R}^2$ (b) Classification by semi-supervised learning and K-means clustering. Test error is 0.0033

For the performance of the semi-supervised learning algorithm, the test error as a function of the number of dimensions the algorithm uses is shown in Fig.9 (a). As the number of dimension goes up, the test error begins to increase. Most of the information is only contained in the first few dimension, and the others contains mainly noise, so there is no advantage of using more dimenstion in the classification algorithm. Fig.9(b) shows the test error as a function of the number of labeled data that the algorithm uses to construct the classifier. As expected, the performance improves when the algorithm uses more labeled data to infer the classifier.

Figure 10 shows the two dimensional mapping of raw SAR data described above. The left image is the result with fully known labels and the right image is the result of classification by semi-supervised learning. We can see there is only one misclassified point in the middle of the image. We have realized, given a specific type of data, that the results were highly dependent on the SNR. The SNR in Figure 10 was 0.07.

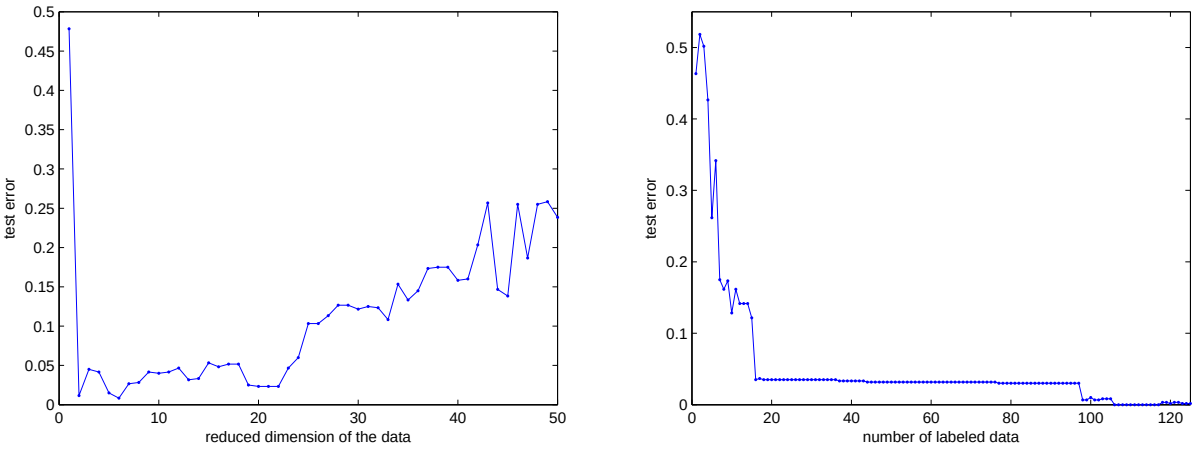

(a) (b)

Fig. 9. Test error. (a) with varying dimension (original dimension : 64×64). (b) with varying number of labeled data (total number of data : 600)

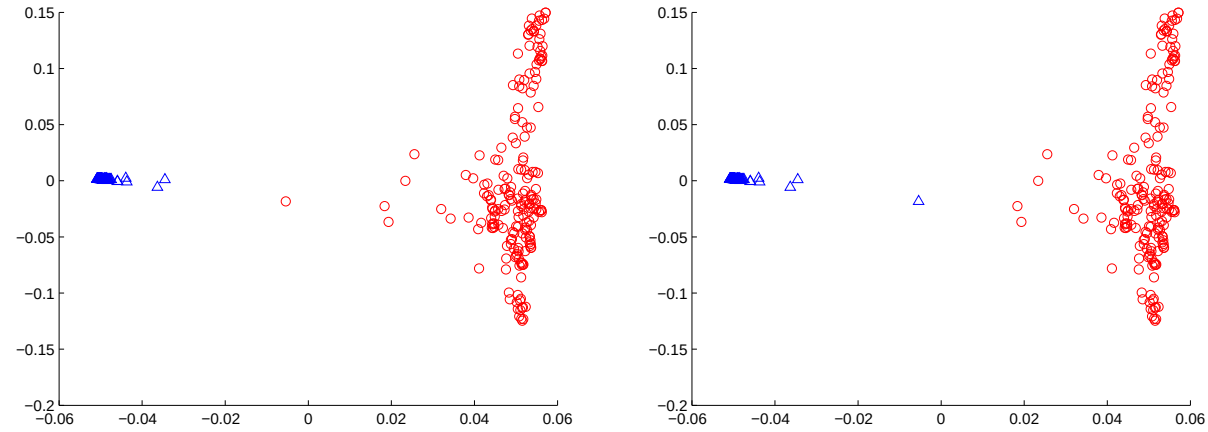

(a) (b)

Fig. 10. Experiment with raw SAR data. (a) Dimension reduced data. (b) Classification by semi-supervised learning

4. DISCUSSION AND FUTURE WORKS

4.1. Challenges in the Experiments

(a) Model selection problem :
The performance highly depends on the model parameters t and n_n. We have been adjusting the values manually so far, and we would like to come up with a way to automatically choose these values.
(b) Dependence on the similarity between two images :
The algorithm works well for the case where the two images differ a lot, either in the Fourier

coefficients or in the images. However, if the two classes of images are similar in some sense, meaning they look very similar to human eyes such as circles and squares with comparable diameters or horizontal and vertical rectangles that overlap in spatial domain, etc, the algorithm fails.
(c) Limitations in data resources :
We were not able to apply our method to realistic SAR data. Hence, we could not conclude how well our algorithm would work in real situations.

4.2. Discussion on Direct Detection from the Fourier Data

Before applying the Laplacian Eigenmap technique to classify the Fourier data, we wanted to see if there was a much easier and straightforward method that would do the job. We started by simulating to match unknown Fourier data with known patterns of the Fourier data of a specific class of images. By match, we mean calculating correlations (inner products) between the unknown and the known Fourier data. We know the Fourier data and the spatial data have a one-to-one correspondence, so we can first recognize the Fourier data pattern of the object that we are searching for and then try to match it with the unknown Fourier data. If we find that the unknown Fourier data contains the pattern we are look for, then we say there is a match. We tried on a set of images containing only one object, and we tried to identify whether the object is a square or not. It turns out that the magnitude part of Fourier data is easy to identify, but the phase part is difficult to identify. This will be a problem when the object in the spatial domain is shifted from the origin, which corresponds to a linear phase change in the Fourier domain. Therefore, we need a method that can take both the magnitude and phase part into consideration.

4.3. Conclusion

We were able to classify two types of images successfully when each type of images resided on a low dimensional manifold and the two manifolds were not too close. The method also worked well when we applied i.i.d. random phase to each pixel in the images to model the complex-valued reflectivity in SAR, although this meant that the images no longer resided on a low dimensional manifold. We have also experimented with the case where noise was present, and it turned out that the SNR strongly affected the performance of the classification. With the simulated raw SAR data, we were able to distinguish between data corresponding to noisy clutter and data corresponding to small rectangle features on noisy clutter. Thus, instead of performing computationally heavy steps of interpolation and inverse Fourier transform, we could apply the detection algorithm directly to the raw data.

4.4. Future Works

In this report we have used Laplacian Eigenmaps as our primary method for dimensionality reduction. We can try using Principal Component Analysis (PCA), Locally Linear Embedding (LLE) and ISOMAP. Also, we need to develop a method for automatic model selection. Most importantly, we need to acquire real raw SAR data and test them with our method.

5. WORK DIVISION

Hyun Jeong Cho generated the test data, and experimented with dimensionality reduction methods.
Jae Young Park implemented and experimented with the dimensionality reduction methods.
Kuang-Hung Liu implemented the algorithm for classification via semi-supervised learning.

6. REFERENCES

[1] Richard G. Baraniuk and Michael B. k Wakin, "Random projections of smooth manifolds," *Foundations of Computational Mathematics*, June 2007.

[2] D. E. Wahl P. H. Eichel D. C. Ghiglia C. V. Jakowatz, Jr. and P. A. Thompson, *Spotlight-Mode Synthetic Aperture Radar: A Signal Processing Approach*, Kluwer Academic Publishers, Boston, 1996.

[3] Mikhail Belkin and Partha Niyogi, "Laplacian eigenmaps for dimensionality reduction and data representation," *Neural Comput.*, vol. 15, pp. 1373 – 1396, June 2003.

[4] Mikhail Belkin and Partha Niyogi, "Semi-supervised learning on riemannian manifolds," *Machine Learning*, vol. 56, pp. 209 – 239, July 2004.

[5] Richard G. Baraniuk Mark A. Davenport, Michael B. Wakin, "Detection and estimation with compressive measurements," Tech. Rep. TREE 0610, Rice University, November 2006.

[6] Richard Baraniuk, "A lecture on compressive sensing," *IEEE Signal Processing Magazine*, July 2007.

[7] H. Choi M. B. Wakin, D. L. Donoho and R. G. Baraniuk, "The multiscale structure of non-differentiable image manifolds," in *Proc. SPIE Wavelets XI*, July 2005.

[8] Richard G. Baraniuk Chinmay Hegde, Michael B. Wakin, "Random projections for manifold learning," in *Proc. Neural Information Processing Systems*, December 2007.